

# Experimental comparison of Wide Field AO control schemes using the Homer AO bench

Amélie Parisot<sup>1,2</sup> <sup>a</sup>, Cyril Petit<sup>1</sup>, Thierry Fusco<sup>1</sup>, and Jean-Marc Conan<sup>1</sup>

<sup>1</sup> ONERA, DOTA, Unité HRA, 29 avenue de la division Leclerc, 92322 Chatillon, France

<sup>2</sup> Laboratoire d'Astrophysique de Marseille, Pôle de l'Etoile, Site de Château-Gombert, 38 rue Frédéric Joliot-Curie, 13388 Marseille Cedex, France

**Abstract.** Wide Field Adaptive Optics (WFAO) concepts are currently being studied in the perspective of future ELT instrumentation. In that context, the ONERA wide field AO facility (HOMER bench) has been developed. HOMER allows the implementation and comparison of control schemes from the simplest least-square to the optimal Linear Quadratic Gaussian solutions including Pseudo-closed loop approach. After a description of the bench internal calibrations and ultimate performance, all these control schemes are compared experimentally in a Laser Tomography AO configuration.

## 1 Introduction

Wide Field Adaptive Optics (WFAO) concepts, such as Ground Layer AO (GLAO), Laser Tomography AO (LTAO) or Multi-Conjugate AO (MCAO) are currently being studied in the perspective of future ELT instruments. In that context, the experimental validation of the various smart control solutions proposed by several teams in the past years is now essential. The goal is to compare respective performance and robustness in experimental condition, and also to assess their respective calibration issues.

In this paper we present experimental validation and comparison of different control schemes for GLAO and LTAO concepts using the Onera WFAO facility (HOMER bench). Gathering a 3D turbulence generator, two deformable mirrors with variable altitude positions and a PC-based flexible and user-friendly Real Time Computer, HOMER allows the implementation of control schemes from the simplest least-square to the optimal Linear Quadratic Gaussian solutions including Pseudo-Open loop approaches. In part 2 we briefly recall the main equations of these control laws, then in part 3 we describe the HOMER bench. We focus in section 4 on calibration issues and model identification, required for an increase of performance and tomographic control. We investigate in particular identification of relative geometry of wavefront sensors. This identification process leads to a well aligned and calibrated bench on which an implementation of different control laws is then performed. They are tested and compared in term of performance and robustness, results are outlined in section 5.

## 2 Control laws

In this section we recall structures of some of the different control schemes implemented on HOMER. First we focus on the standard and simple approach: a least square estimator associated to an integrator controller. Then we present two tomographic control laws: the Pseudo Open Loop Control (POLC) and the Linear Quadratic Gaussian (LQG) solution.

### 2.1 Least Square estimator plus Integrator

The least square estimator is a common approach.

---

<sup>a</sup> amelie.parisot@onera.fr

## AO for ELT II

We assume that the Deformable Mirror (DM) control voltages space is linked to the Wave-Front Sensor (WFS) slope measurements space through a linear operator which can be defined as

$$M_{int} = DN \quad (1)$$

where  $M_{int}$  is the interaction matrix,  $D$  is the WFS matrix and  $N$  is the DM influence matrix. The command matrix is simply the pseudo inverse of the interaction matrix:

$$M_{com} = ((M_{int})^T M_{int})^\dagger (M_{int})^T. \quad (2)$$

The control voltages at time  $n$   $u_n$  are calculated thanks to an integrator controller [1] with a gain  $g$ :

$$u_n = u_{n-1} + g.M_{com}y_n. \quad (3)$$

This common solution is robust, and its stability is ensured by the choice of  $g$ . Nonetheless it has no tomographic capabilities, correction is suboptimal.

### 2.2 Pseudo Open Loop Control

The Pseudo Open Loop Control (POLC) [2] is based on the tomographic minimum mean square error estimator (MMSE) [3]. MMSE estimator considers a static open-loop system, to circumvent this limitation POLC approach takes into account that the system is dynamic and closed loop: DM correction effect is subtracted to measurements in order to apply the MMSE to these calculated pseudo open loop measurements. An Infinite Input Response (IRR) filter is applied to handle temporal dynamics. The main operations are thus:

- Reconstruction of the pseudo open loop measurements  $y_n^{ol}$ :

$$y_n^{ol} = y_n + M_{int}u_{n-2} \quad (4)$$

- Turbulence estimation and comparison with the previous estimated one to derive an error terme  $e_n$ :

$$e_{n-1} = R^{mmse}y_n^{ol} - \hat{\varphi}_{n-1}^{tur} \quad (5)$$

- Prediction of the phase through a temporal filter:

$$\hat{\varphi}_{n+1}^{tur} = \alpha\hat{\varphi}_n^{tur} + \gamma\hat{\varphi}_{n-1}^{tur} + \delta e_{n-1} \quad (6)$$

- Computation of the corrective control voltages by a least square projection (assuming that the DM is linear and has no temporal dynamics):

$$u_n = P\hat{\varphi}_{n+1}^{tur} \quad (7)$$

where  $P$  is the least-square projector from the phase in the turbulent layers in the direction of interest to the DM space.

Though suboptimal this approach provides efficient tomographic reconstruction in closed-loop system, with account of temporal dynamics, and it is being studied in the Thirty Meter Telescope framework.

### 2.3 Linear Quadratic Gaussian control

LQG approach has been proposed for AO systems from the early 90's [4]. It is the optimal solution with respect to minimum residual phase variance of the dynamic closed-loop control problem. In this section we only recall the main equations and important points. More details about the formalism can be found in [5] and [6].

LQG relies on priors on spatial and temporal characteristics of the turbulence.

It is assumed that the atmosphere can be modeled by  $L$  discrete turbulent layers statistically independent. Each layer  $i$  is characterised by its altitude  $h_i$ . Considering a maximal Field Of View (FoV)  $\theta$ ,  $\varphi_{i,n}^{tur}$  is the average turbulent phase on interval  $[(n-1)T, nT]$  in the layer  $i$ , corresponding to the discrete instant  $n$ .

A turbulent phase in the volume  $\varphi_n$  is defined by the concatenation of the turbulent phases of each layer  $i$ . Considering several analysis directions  $\alpha$ , the turbulent phase seen in the telescope pupil is equal to  $\phi_{\alpha,n}^{tur} = M_{\alpha}^L \varphi_n^{tur}$ , where  $M_{\alpha}^L$  is a linear operator performing the sum of all contributions of each turbulent layer ( $L$ ) in all directions  $\alpha$ . The correction phase in the directions  $\beta$  in the pupil is then given in a similar way by  $\phi_{\beta,n}^{corr} = M_{\beta}^M \varphi_n^{corr}$ , for a configuration using  $M$  DMs for correction.

Considering  $n_{gs}$  guide stars and directions of analysis  $\alpha$  and  $n_{obj}$  objects of interests with directions of interest  $\beta$ , the residual wave front measurement  $y_n$  obtained in directions  $\alpha$  is:

$$y_n = D (M_{\alpha}^L \varphi_{n-1}^{tur} - M_{\alpha}^M N u_{n-2}) + w_n. \quad (8)$$

The measurement noise  $w_n$  is a generalised measurement noise vector for all WFSs.

The residual phase in directions of interest  $\beta$  is given by:

$$\phi_n^{res} = M_{\beta}^L \varphi_n^{tur} - M_{\beta}^M N u_{n-1}. \quad (9)$$

The MCAO optimality criterion is obtained as the generalisation of the AO criterion [7] which aims at minimising the residual phase variance in a given FoV:

$$J(u)^{mcao} = \lim_{n \rightarrow +\infty} \frac{1}{n} \sum_{j=1}^n \|M_{\beta}^L \varphi_j^{tur} - M_{\beta}^M N u_{j-1}\|^2. \quad (10)$$

The solution of the control problem in equation (10) is a two step resolution. This classic result is known as the stochastic separation theorem [8,9] and states that the optimal control  $u_n$  can be constructed by separately solving a deterministic control problem and a stochastic minimum variance estimation problem.

The stochastic minimum variance estimation problem consists in estimating and predicting the turbulent phase. Its solution is provided, in the linear gaussian case, by the Kalman filter. To describe the LQG control, a state-space representation of the system is usually specified. For a simple turbulent phase model of the form  $\varphi_{n+1} = A_{tur} \varphi_n + \nu_n$ , a state-space model can be defined as in [6]. A higher order model of turbulence estimation can also be considered, but no significant increase of performance has been obtained on the HOMER bench. All the matrices of the state-model being stationary, the asymptotic formulation of the Kalman filter is applied. The estimate  $\hat{\varphi}_{n/n}$  of the turbulent phase  $\varphi_n$  and the prediction of the turbulence  $\hat{\varphi}_{n+1/n}^{tur}$  can be found in [6]. The LQG optimal control comes down to the following and compact form:

- Estimation of the phase  $\hat{\varphi}_{n/n}$

$$\hat{\varphi}_{n/n} = \hat{\varphi}_{n/n-1} + H_{\infty} (y_n - D M_{\alpha}^L \hat{\varphi}_{n-1/n-1}) \quad (11)$$

where  $H_{\infty}$  is the asymptotic Kalman gain.

- Prediction of  $\hat{\varphi}$

$$\hat{\varphi}_{n+1/n} = A_{tur} \hat{\varphi}_{n/n} \quad (12)$$

- Computation of the corrective control voltages by a least square projection (assuming that the DM is linear and has no temporal dynamics):

$$u_n = P \hat{\varphi}_{n+1/n}. \quad (13)$$

LQG approach provides the optimal solution, it has been numerically and experimentally validated [6]. But validation in more realistic conditions has to be performed, and studies on parameters optimisation and robustness are being carried out.

### 3 Homer bench layout

HOMER bench is a laboratory bench devoted to implementation and validation of WFAO concepts such as GLAO, LTAO or MCAO. A detailed description can be found in [10].

Figure 1 shows on the left a picture of the HOMER bench and its main components and on the right the optical layout.

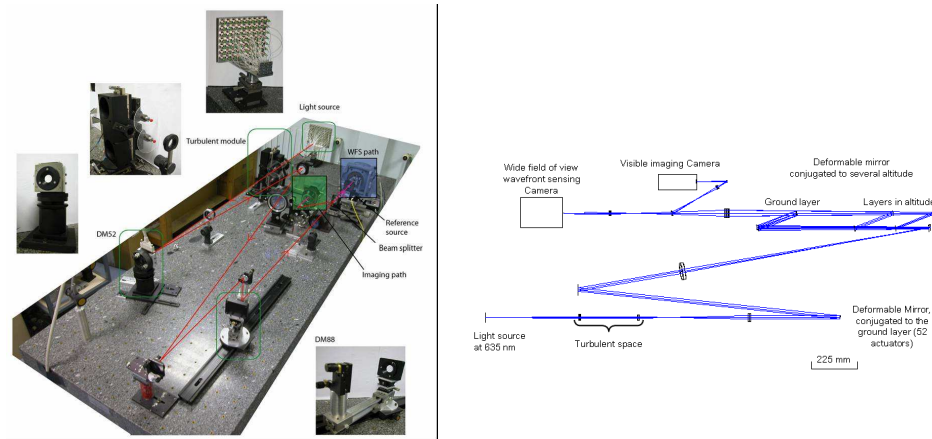


**Fig. 1.** Left: Picture of the bench and its main components. Right: Optical layout of HOMER.

The source module is made up with  $7 \times 9$  unresolved sources in the visible wavelengths ( $\lambda = 635 \pm 5$  nm) dispatched over a reconfigurable cartesian grid. This leads to a field of view of  $427\lambda/D * 484\lambda/D$ . The source module is associated with a collimator  $D_s$  to simulate Natural Guide Stars (NGS).

Then light comes through three Kolmogorov type turbulent layers on a rotating stage. A wide field WFS analyses GS.s light. It is a Shack-Hartmann based WFS, made up of a  $7 \times 7$  sub-aperture lenslet array (37 effective sub-pupils) and of an ANDOR iXon DU895LC camera, which is a low noise EMCCD with  $1004 \times 1002$  pixels of  $8 \mu\text{m}$ . A distinctive feature of HOMER design is that a single wide field Shack Hartmann WFS is used: each sub-aperture can see a field of view equal to  $FoV = 427\lambda/D$ , corresponding to  $142 \times 142$  pixels on the EMCCD detector (at Shannon sampling). Wavefront sensing is performed on up to 5 regions (this number can be extended, it depends on RTC memory size) by numerical windowing around each selected GS. This single WFS configuration allows to easily change the number and the configuration of the GSs while it reduces the calibration and synchronisation issues.

Correction is performed with two magnetic membrane DM from ALPAO firm<sup>1</sup>. In this article, we consider only the first DM, DM1, conjugated with the pupil, the second one is replaced by a flat mirror. DM1 has 52 effective actuators, for a 17.5 mm diameter. A wide field imaging camera is used for performance computation.

The whole system assembly is controlled using a Linux PC RTC from the SHAKTIWARE company<sup>2</sup>, working at around  $F_{ech} = 12$  Hz. This limited frequency is due to the WFS camera frames transfer. However the ratio  $V/(DF_{ech})$ , where  $V$  is the wind speed and  $D$  the pupil diameter is representative of a VLT case.

Apart from the classic integrator control law, various control laws can be implemented on the RTC. Indeed, any control law that can be written in the form:

<sup>1</sup> more details on ALPAO DM can be found on their web site [www.alpao.com](http://www.alpao.com)

<sup>2</sup> more details on Shaktiware company can be found on their web site [www.shaktiware.com](http://www.shaktiware.com)

$$\begin{aligned} X_{n+1} &= M_1 \cdot X_n + M_2(y_n + M_3 \cdot u_{n-2}) \\ U_n &= M_4 X_{n+1} \end{aligned}$$

may be implemented on the RTC, as long as matrices  $M_1, M_2, M_3$  and  $M_4$  are defined by the user. This generic expression of the control law allows to implement LQG but also POLC, classic integrator etc.

## 4 Identification of the mismatch WFS/DM

Several parameters may not be well calibrated when the bench is aligned, such as translation between the DM and the WFS, or the direction of analysis and correction of the turbulence. These miscalibrations could have significant effects depending of the implemented control law. The LSE approach directly relies on the interaction matrix, and POLC and LQG approaches rely on models of the components. Thus, a system parameter identification process has been set up, based on a minimisation algorithm using the interaction matrix as input data, as it is the usual calibrated element which contains misalignment information.

In this article, we focus on the identification of the residual mismatch between the DM and the WFS. It can be described by 4 parameters: two orthogonal translations  $x_0, y_0$ , a rotation  $\theta$ , and a magnification  $g_y$  due to a conjugation error.

Sensitivity of the system performance to misalignment and calibration errors affecting all these parameters will depend on the system itself. A numerical analysis has been performed on the impact of a WFS/DM mismatch on HOMER performance for the different control laws. For example in a LSE case, it leads to the following tolerances:

- relative translation between DM and WFS is acceptable up to 1/7 of a sub-aperture,
- relative rotation between DM and WFS is acceptable up to 1/7 of an edge sub-aperture,

The required precision for HOMER is not very challenging because of the high DM coupling factor and the low number of actuators. But the developed identification process can be applied to more demanding systems, such as SAXO, the XAO system of SPHERE [11]. Its specification on DM/WFS alignment is 1/10 sub-aperture.

Parameters of interest will be identified thanks to an iterative comparison between the experimental matrix and the estimated one. A multi-variable minimisation algorithm is used to perform the estimation (Levenberg-Marquardt type algorithm [12] in our case).

After a numerical validation, the identification algorithm has been validated on HOMER bench. A known mismatch is introduced in translating and/or rotating the microlens matrix of the WFS, so it can be precisely calibrated thanks to the WFS slopes, at high Signal to Noise Ratio (SNR). Since subapertures have 142\*142 pixels, and since error on slopes is 1/10 pixel, the precision is better than 1/1000 subaperture. For each position, 10 matrices are computed in 3 different SNR conditions. A joint estimation of the relative translation, the relative rotation and the magnification is then performed using the method. SNR is here defined as  $SNR = \max(M_{int}) / \sigma(M_{int}(\text{unused} - \text{subpup}))$

The results shown in figure 2 present the performance achieved by the algorithm in the translation and the rotation estimation, for the 3 SNR conditions. For translations lower than 0.5 sub-aperture, the precision is better than 1/100 subaperture, and even for poor SNR condition, it is better than 1/20 subaperture. Performance achieved for rotation estimation is the same. The identified magnification is uniform =0.088. It is worth noting that performance is the same for a misregistration composed of a X-Y translation plus a rotation.

This identification process gives precision that is far beyond the required one. It can be used for re-alignment of the system and for refining models used in tomographic control laws. The next step will be to validate it on a more challenging and real system.

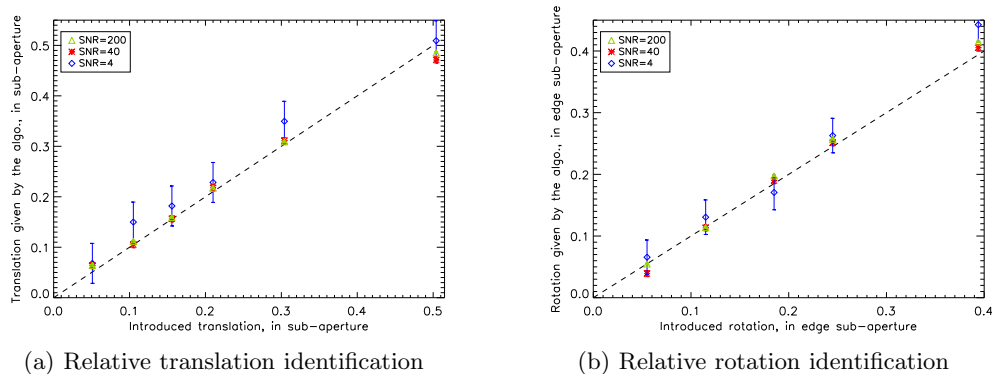


**Fig. 2.** Experimental results of estimation of the relative translation and rotation between the WFS and the DM in the pupil on HOMER bench. Three SNR cases are tested. Error bars represent  $\pm$  the standard deviation of the estimated value for a population of 10  $M_{int}$ . Error bars on the introduced mismatch is  $\pm 1/1000$  sub-aperture, so this error is negligible.

## 5 WFAO control schemes experimental results

In this section we present the experimental validation on HOMER of different control schemes in a LTAO configuration. The bench has been precisely re-aligned by using the identification process described in part 4.

### 5.1 Experimental conditions

We perform analysis on the central GS in AO and on four GSs in TAO. In both cases correction is optimised for the central star and only natural guide stars are used. Three fields of view are considered: a narrow field of view where the FoV radius is  $18''$ , a medium FoV which the radius is  $36''$  and a large FoV which the radius is  $54''$ . The relative separation between a GS footprint and the central star footprint  $\delta$  is respectively 11%, 22%, 33% at 10000 m.

Turbulence is generated with three layers, their parameters in a VLT-equivalent case are gathered in table 1. This turbulent system corresponds to a  $D/r_0$  of 8.

Layer number	1	2	3
Altitude(m)	0	5000	10000
$C_n^2$ fraction	0.52	0.32	0.16
Wind speed ( $m.s^{-1}$ )	9	5	20

**Table 1.** Turbulence parameters used in simulation and on the bench (VLT-equivalent case).

Correction is performed by the ground DM. Three control schemes have been studied:

- classic controller, which is a least-square plus a simple integrator. The single global gain is optimised for each configuration
- POLC, which estimates the three layers of turbulence with the exact profile, on respectively [74, 84, 90] Zernike modes for the narrow FoV, [74, 93, 106] for the medium FoV and [74, 103, 122] for the large FoV (in the ratio of metapupils diameters).  $\alpha$  and  $\gamma$  are set to 0.495.
- LQG, which also estimates the three turbulent layers, with the same number of Zernike modes as in a POLC case.

## 5.2 Results on HOMER

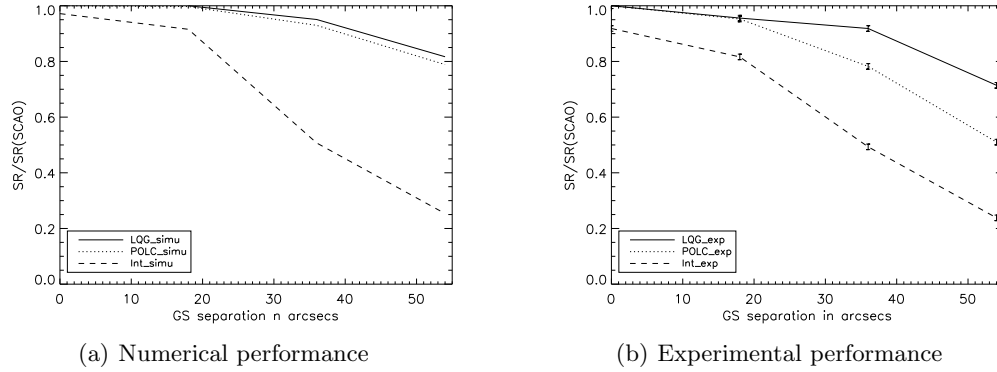


**Fig. 3.** Compared performance of LSE (dashed line), POLC (dotted line) and LQG (solid line) with respect to the FoV radius in high SNR conditions.

Figure 3(b) shows the normalised performance of correction on the central star according to the angular separation between GSs and the central star. The normalised performance is the ratio between the Strehl Ratio (SR) and the SR obtained in classical AO in LQG. We also present on figure 3(a) the normalised performance obtained with the end-to-end simulation of HOMER. First, we clearly see the gain obtained in performing tomographic estimation for all the FoV. Figure 4 shows the Strehl map in the widest FoV configuration. Note that the SR in SCAO is 29%. Compared with the integrator solution SR is doubled with the POLC solution and trebled with the LQG solution.

The simple integrator experimental results and numerical results tally, so it assures we have a good simulation of HOMER. On the other hand, the gap between experimental and numerical results in POLC and LQG widens with the GSs angular distance. However the difference is equal to 12% in a LQG case compared to 35% for a POLC control. This latter seems to be more sensitive to model errors. Simulations to compare robustness to model errors will be done to confirm this point.

For an equivalent on-line complexity, POLC appears to be less robust to model errors.

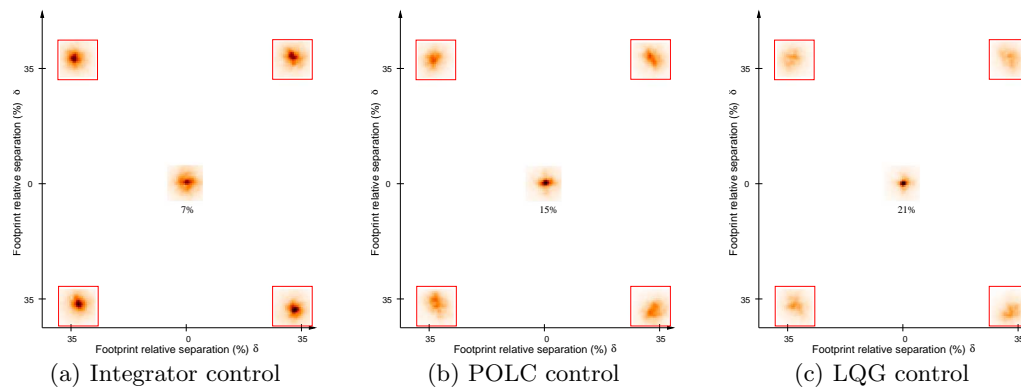


**Fig. 4.** Experimental long-exposure PSFs obtained with different control laws. The GSs are surrounded by a red solid square.

## 6 Conclusions

The HOMER bench is now a calibrated WFAO bench on which implementation and comparison of various control schemes can be done. An identification process of system parameters has been developed in order to precisely re-align the bench and to get more accurate model for tomography. This process has been validated on HOMER and it has given very good results, far beyond the HOMER requirements. The next step will be to test it on a real system with very strong requirements such as the SPHERE XAO bench. After having carefully aligned and calibrated the HOMER bench we have implemented and compared various WFAO control laws (integrator, POLC and LQG control schemes). Preliminary results seem to confirm the efficiency and robustness of LQG control with respect to model errors. End to end simulations nicely fit experimental results and will be used to extensively analyse and interpret the bench measurement. We can also implement other control laws such as Virtual DM approach [13], or Simple Matrix Vector Multiplication solutions derived from tomographic control laws, such as Degraded LQG [14].

## References

1. F. Roddier, *Adaptive Optics in Astronomy* (Cambridge University Press, 1999)
2. L. Gilles, *Closed-loop stability and performance analysis of least square and minimum-variance control algorithms for multi-conjugate adaptive optics* Applied Optics **44,6**, pp.993-1002 (2005)
3. E.P. Wallner, *Optimal wave-front correction using slope measurements* JOSA A. **73**, pp.1771-1776 (1983)
4. R.N. Paschall, D.J. Anderson, *Linear Quadratic Gaussian control of a deformable mirror adaptive optics system with time-delayed measurements*, Applied Optics, **32** 6347-6358 (1993)
5. B. Leroux, J-M. Conan, C. Kulcsár, H-F. Raynaud, L. Mugnier, T. Fusco *Optimal control law for classical and multiconjugate adaptive optics* JOSA A. **21**, pp.1261-1276 (2004)
6. C. Petit, J-M. Conan, C. Kulcsár, H-F. Raynaud, *Linear quadratic gaussian control for adaptive optics and multiconjugate adaptive optics: experimental and numerical analysis* JOSA A. **26**, pp.1307-1325 (2009)
7. C. Kulcsár, H-F. Raynaud, C. Petit, J-M. Conan, P. Viaris de Lesegno *Optimal control, observers and integrators in adaptive optics*, Optics Express, **14**, 7464-7476 (2006)
8. P. Joseph, J. Tou, *On linear control theory*, AIEE Trans. on Appl. and Indus **80**, pp.193-196 (1961)
9. Y. Bar-Shalom, E. Tse, *Dual effect, certainty equivalent and separation in stochastic control*, IEEE Trans. Automat. Contr, **19**, pp.494-500 (1974)
10. A. Costille, C. Petit, J-M. Conan, C. Kulcsar, H-F. Raynaud, T. Fusco, *Wide field adaptive optics laboratory demonstration with closed loop tomographic control*, JOSA A. **27**, pp.469-483 (2010)
11. T. Fusco, G. Rousset, J.-F. Sauvage, C. Petit, J.-L. Beuzit, K. Dohlen, D. Mouillet, J. Charton, M. Nicolle, M. Kasper, P. Baudoz, P. Puget, *High-order adaptive optics requirements for direct detection of extrasolar planets: Application to the SPHERE instrument*, Optics Express **14**, 7515-7534 (2006)
12. Donald W. Marquardt, *An algorithm for least-squares estimation of nonlinear parameters*, Journal of Optical Society for Industrial and Applied Mathematics, **11**, pp.431-441 (1963)
13. M. Le Louarn, *Multi-Conjugate Adaptive Optics with laser guide stars: performance in the infrared and visible*, Monthly Notices of the Royal Astronomical Society, **334**, Issue 4, pp. 865-874 (2002)
14. C. Petit, M. le Louarn, T. Fusco, P.-Y. Madec, *Efficient control schemes with limited computation complexity for tomographic AO systems on VLTs and ELTs*, AO4ELT2 (2011)